Measurement of two-qubit states with quantum point contacts coupled by a quantum dot

2005 J. Phys.: Condens. Matter 17 6895

(http://iopscience.iop.org/0953-8984/17/43/009)

INSTITUTE OF PHYSICS PUBLISHING JOURNAL OF PHYSICS: CONDENSED MATTER

J. Phys.: Condens. Matter **17** (2005) 6895–6909 doi:10.1088/0953-8984/17/43/009

Measurement of two-qubit states with quantum point contacts coupled by a quantum dot

Tetsufumi Tanamoto[1] **and Xuedong Hu**[2]

[1] Corporate R&D Center, Toshiba Corporation, Saiwai-ku, Kawasaki 212-8582, Japan
[2] Department of Physics, University at Buffalo, SUNY, Buffalo, NY 14260-1500, USA

E-mail: tetsufumi.tanamoto@toshiba.co.jp

Received 14 June 2005, in final form 18 August 2005
Published 14 October 2005
Online at stacks.iop.org/JPhysCM/17/6895

Abstract

We solve the master equations of two charge qubits measured by two serially coupled quantum point contacts (QPCs). We describe two-qubit dynamics by comparing entangled states with product states, and show that the QPC current can be used for reading out results of quantum calculations and providing evidences of two-qubit entanglement. We also calculate the concurrence of the two qubits as a function of dephasing rate that originates from the measurement. We conclude that coupled charge qubits can be effectively detected by a QPC-based detector.

(Some figures in this article are in colour only in the electronic version)

1. Introduction

Quantum information processing in charge-based solid state nanostructures has attracted widespread attention because of the potential scalability of such devices, and the relative ease with which such charge devices can be manipulated and detected [1–4]. Recently, two-qubit coherent evolution and possibly entanglement have been observed in capacitively coupled Cooper pair boxes [5]. For universal quantum computing, two-qubit operations are required, so the realization of controlled two-qubit entanglement is regarded as a crucial milestone for the study of solid state quantum computing. While two-qubit information can be detected with one measurement device on each qubit, it is also important to search for a detector that is directly sensitive to two-qubit information, and to develop a proper formalism to study two-qubit measurement processes [6–8].

The ultimate criterion for the detection of qubits is whether we can distinguish the results of a quantum computation by the output signal of the detector, e.g. current or conductance of a single electron transistor. In the case of one qubit, two single-qubit states $|\downarrow\rangle$ and $|\uparrow\rangle$ need to be distinguished. In the case of two qubits, four two-qubit state, $|\downarrow\downarrow\rangle$, $|\downarrow\uparrow\rangle$, $|\uparrow\downarrow\rangle$, and $|\uparrow\uparrow\rangle$ (we will call them $|A\rangle \sim |D\rangle$) need to be distinguished before the qubit states are destroyed by the measurement. As we mentioned above, measurement of multi-qubit states can generally be achieved by multiple single-qubit measurements on each of the qubits, respectively. Here we

study a different detection process: the temporal behaviour of a detector (QPC in the present study) that simultaneously couples to two qubits. We show that information contained in the temporal evolution of the QPC current can help us distinguish different two-qubit product states, and some entangled states from the product states. Indeed, one motivation of our study is to obtain direct evidence for the entanglement of the qubits, possibly from the detector current or other measurable quantities.

In [8], we studied a particular scheme for the quantum measurement of two charge qubits by a two-island single-electron transistor (SET), and showed that the SET is an effective detector of the two-charge-qubit states. Here the charge qubits are constituted of two coupled quantum dots (QDs) with one excess electron. Due to tunnel coupling of the QDs, the wavefunctions in a qubit are superpositions of localized states from each of the QDs. If a qubit is prepared in a single QD state, it tends to oscillate between the two sides of the double QD. If we define the local states as $|\uparrow\rangle$ and $|\downarrow\rangle$, the qubit state oscillates between the two logical states with a frequency determined by the tunnelling coupling and the difference of the energy levels of the two QDs. Time-dependent behaviour of this coherent oscillation of the qubits is determined by the initial state. If we take the initial time to be that when a final quantum operation is applied to the qubit, the detector readout current reflects the results of quantum calculation. The qubit states interact with the readout current by changing the energy (and therefore occupation) of the electronic states in the SET islands and possibly the tunnelling rates of the junctions (by modifying the island electronic states themselves) on both sides of the islands. Although, in [8], we show that the SET can distinguish the different coherent oscillations between the two-qubit product states and the entangled states, we have not yet investigated the two-qubit dynamics itself.

Here we would like to study quantum point contact (QPC) as a detector for two coupled charge qubits (figure 1). A QPC is essentially a one-dimensional conducting channel and is considered to be an effective charge detector, similar to the SET. The particular scheme we consider consists of two low-transparency QPCs connected in series through a single level quantum dot. Each of the QPCs, which in this paper simply represents tunnel coupling between two conducting regions, is close to a charge qubit so that its current is dependent on the state of the respective qubit. In order to take into account an interaction between qubits, the distance between the two qubits should be small; thus it would be natural that the region between the two QPCs is also sufficiently small such that its energy level is quantized (figure 2). We include an on-site Coulomb interaction in our study to describe the Coulomb blockade effect in the inter-QPC island.

Compared to the SET detector, the QPC detector interacts with qubits only through the change of tunnelling rates. Although the SET detector is able to describe a variety of features of the internal states of qubits in [8], we could not identify which of the two interactions (that between the islands and qubits, which modify the level occupations on the SET islands; or that between the tunnelling junctions and qubits, where potential by the qubits modifies the tunnelling rates) plays the major role in the SET detector. Thus, an important question is whether or not the QPC detector that interacts with qubits only by the change of the tunnelling rates is also an effective apparatus for detecting the qubit states. In this paper, after discussing the basic two-qubit dynamics with no detector, we focus mainly on the following issues:

(1) whether we can distinguish the four product states $|A\rangle \sim |D\rangle$ of two coupled charge qubits in the time-domain with a serially coupled QPC detector,
(2) whether we can distinguish the entangled states from the product states of these two qubits, and
(3) whether the quantum Zeno effects in the coupled charge qubits can be observed.

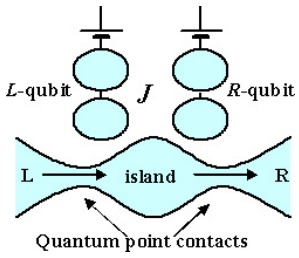

Figure 1. Two charge qubits (using double quantum dot charged states) are capacitively coupled to a detector of two serially coupled QPCs. J is the strength of inter-qubit interaction. No tunnelling is allowed between the QPC detector and any of the qubits.

Figure 2. Electronic states in the inter-QPC island. We assume that there is only one accessible electronic orbital state on the island. There are thus in total four possible island states: (a) empty dot—state 'a' has no excess electron on the dot. (b) Single-electron dot—state 'b' has one electron with spin up or down. (c) Two-electron dot—state 'c' has two electrons in a spin singlet state occupying the same orbital state.

In the following sections, we solve the master equations for the coupled qubit–QPC system and investigate the effectiveness of the proposed QPC detector. In section 2, we present our formulation of two qubits and the QPC detector. In section 3, we discuss the difference between the dynamics of a single qubit and that of two qubits. In section 4, we show the numerical results of two-qubit detection by QPC. Section 5 is devoted to a discussion of QPC detection, and section 6 consists of a conclusion.

2. Formulation

In the present measurement scheme, the QPCs are capacitively coupled to the charge qubits (figure 1), so the current through them sensitively depends on the states of the qubits. We describe the two QPCs using two tunnel matrix elements only and neglect further internal structures [9]. We assume that the qubit–QPC coupling is purely capacitive, so there is no current flowing from the qubits to either of the QPC electrodes. The Hamiltonian for the combined two qubits and the QPCs is written as $H = H_{\rm qb} + H_{\rm qpc} + H_{\rm int}$. $H_{\rm qb}$ describes the two interacting qubits (left and right, as illustrated in figure 1), each consisting of two tunnel-coupled QDs and one excess charge [6]:

$$H_{\rm qb} = \sum_{\alpha={\rm L,R}} (\Omega_\alpha \sigma_{\alpha x} + \Delta_\alpha \sigma_{\alpha z}) + J\sigma_{{\rm L}z}\sigma_{{\rm R}z}, \tag{1}$$

where Ω_α and Δ_α are the inter-QD tunnel coupling and energy difference (gate bias) within each qubit. Here we use the spin notation such that $\sigma_{\alpha x} \equiv a_\alpha^\dagger b_\alpha + b_\alpha^\dagger a_\alpha$ and $\sigma_{\alpha z} \equiv a_\alpha^\dagger a_\alpha - b_\alpha^\dagger b_\alpha$ ($\alpha = {\rm L, R}$), where a_α and b_α are the annihilation operators of an electron in the upper and lower QDs of each qubit. Thus, $|\uparrow\rangle$ and $|\downarrow\rangle$ refer to the two single-qubit states in which the excess charge is localized in the upper and lower dot, respectively. J is a coupling constant between the two qubits, originating from capacitive couplings in the QD system [6].

The two serially coupled QPCs are described by $H_{\rm qpc}$:

$$H_{\rm qpc} = \sum_{\substack{\alpha={\rm L,R}\\ s=\uparrow,\downarrow}} \sum_{i_\alpha} \left[E_{i_\alpha} c_{i_\alpha s}^\dagger c_{i_\alpha s} + V_{i_\alpha s}(c_{i_\alpha s}^\dagger d_s + d_s^\dagger c_{i_\alpha s}) \right] + \sum_{s=\uparrow,\downarrow} E_{\rm d} d_s^\dagger d_s + U d_\uparrow^\dagger d_\uparrow d_\downarrow^\dagger d_\downarrow. \tag{2}$$

Here $c_{i_{\rm L}s}(c_{i_{\rm R}s})$ is the annihilation operator of an electron in the $i_{\rm L}$th ($i_{\rm R}$th) level ($i_{\rm L}(i_{\rm R}) = 1,\ldots,n$) of the left (right) electrode, d_s is the electron annihilation operator of the island between the QPCs, $E_{i_{\rm L}s}(E_{i_{\rm R}s})$ is the energy level of electrons in the left (right) electrode, and $E_{\rm d}$ is that of the island. Here we assume only one energy level on the island between the two QPCs, with spin degeneracy. $V_{i_{\rm L}s}$ ($V_{i_{\rm R}s}$) is the tunnelling strength of electrons between the left (right) electrode state $i_{\rm L}s$ ($i_{\rm R}s$) and the island state. U is the on-site Coulomb energy of double occupancy in the island. Note that the number of island states here (figure 2) is much smaller than that of the two-island SET states [8], where we need to take into account at least ten types of detector states. In [8], we observed that the two-island SET can represent a variety of qubit states because of its large number of degrees of freedom. With a much simpler state structure for the present coupled QPC scheme, we will study whether the QPC current could still represent the qubit states with sufficient clarity.

The capacitive interaction between the qubits and the QPCs is represented by $H_{\rm int}$, which contains the information that localized charge near the QPCs increases the energy of the system electrostatically, thus affecting the tunnel coupling between the QPCs and the island in between [10]:

$$H_{\rm int} = \sum_{\alpha={\rm L,R}} \sum_{i_\alpha,s} \delta V_{i_\alpha s}(c^\dagger_{i_\alpha s} d_s + d^\dagger_s c_{i_\alpha s})\sigma_{\alpha z}, \tag{3}$$

where $\delta V_{i_\alpha s}$ is an effective change of the tunnelling strength between the electrodes and QPC island (we shift the origin of the interaction energy such that $\delta V_{i_\alpha,s} = 0$ corresponds to the case where qubits are not polarized $\sigma_{\alpha z} = 0$). We assume that the tunnelling strength of electrons weakly depends on the energy $V_{i_\alpha s} = V_\alpha(E_{i_\alpha s})$ and electrodes are degenerate up to the Fermi surface. Then the qubit–QPC interaction dictates that qubit states influence the QPC tunnelling rate in the form of $\Gamma^{(\pm)}_\alpha(E) \equiv 2\pi\wp_\alpha(E)|V^{(\pm)}_\alpha(E)|^2$ and $\Gamma^{(\pm)'}_\alpha(E) \equiv 2\pi\wp_\alpha(E+U)|V^{(\pm)}_\alpha(E+U)|^2$, where $V^{(\pm)}_\alpha(E) = V_\alpha(E) \pm \delta V_\alpha(E)(\delta V_\alpha(E) > 0)$, and $\wp_\alpha(E)$ is the density of states of the electrodes ($\alpha = {\rm L,R}$). Hereafter, we use $\Gamma^{(\pm)}_\alpha$s and $\Gamma^{(\pm)'}_\alpha$s estimated at the Fermi energy μ_α of the electrodes to describe the tunnelling rate in the detection process of the qubit states by the two QPCs. This is reasonable from a practical standpoint since many experiments are described using Γ_α [1, 3]. The values of the corresponding $\Gamma^{(\pm)}_\alpha$ s are determined by the structure of the system such as the distance between the qubits and the QPCs. For example, a $|{\downarrow}\rangle$ state ($|{\uparrow}\rangle$ state) in a qubit means the excess charge is localized in the lower (upper) dot, so the corresponding tunnelling rate should be $\Gamma^{(-)}_{\rm L}$ ($\Gamma^{(+)}_{\rm L}$). Therefore, two-qubit state $|A\rangle$ would lead to QPC tunnelling rates of ($\Gamma^{(-)}_{\rm L}$, $\Gamma^{(-)}_{\rm R}$) or ($\Gamma^{(-)'}_{\rm L}$, $\Gamma^{(-)'}_{\rm R}$), depending on whether or not the island between the QPCs is doubly occupied. Similarly, $|B\rangle$, $|C\rangle$ and $|D\rangle$ states correspond to ($\Gamma^{(-)}_{\rm L}$, $\Gamma^{(+)}_{\rm R}$) (or ($\Gamma^{(-)'}_{\rm L}$, $\Gamma^{(+)'}_{\rm R}$)), ($\Gamma^{(+)}_{\rm L}$, $\Gamma^{(-)}_{\rm R}$) (or ($\Gamma^{(+)'}_{\rm L}$, $\Gamma^{(-)'}_{\rm R}$)), and ($\Gamma^{(+)}_{\rm L}$, $\Gamma^{(+)}_{\rm R}$) (or ($\Gamma^{(+)'}_{\rm L}$, $\Gamma^{(+)'}_{\rm R}$)), respectively.

We construct the equations for the qubit–QPC density matrix elements at zero temperature $T = 0$, similar to [8]. This method is applicable when the energy level of the inter-QPC island is in between the chemical potentials of the two electrodes. The wavefunction $|\Psi(t)\rangle$ of the qubit–QPC system can be expanded over the Hilbert space spanned by the two-electron states of the qubits, the island states of the QPC shown in figure 1, and all possible electrode states. We choose $|0\rangle$ to refer to the initial ground state of the whole detector system (two electrodes and the inter-QPC island) where the two electrodes are filled with electrons up to $\mu_{\rm L}$ and $\mu_{\rm R}$, respectively, and the two QPCs and the inter-QPC island are empty of excess electrons. The basis states for the QPC can then be constructed from $|0\rangle$ by moving electrons from the left electrode (with higher chemical potential) to the inter-QPC island and the right electrode. We categorize the detector states by the number of electrons that are transferred from the left to

the right electrode (figure 1):

$$|\Psi(t)\rangle = |\Psi_0(t)\rangle + |\Psi_1(t)\rangle, \tag{4}$$

where $|\Psi_0(t)\rangle$ is the part of the wavefunction that no electron tunnels through to the right electrode and $|\Psi_1(t)\rangle$ represents the part of the wavefunction where one or more electrons are transferred to the right electrode. $|\Psi_0(t)\rangle$ can be expressed as

$$|\Psi_0(t)\rangle = \sum_{z_0=A,B,C,D} \left\{ b^{(0)a,z_0}(t) + \sum_{ls} b_{ls}^{(0)b,z_0}(t) d_s^\dagger c_{ls} + \sum_{l_1 l_2} b_{l_1 l_2 \uparrow\downarrow}^{(0)c,z_0}(t) d_\uparrow^\dagger d_\downarrow^\dagger c_{l_1\uparrow} c_{l_2\downarrow} \right\} |0\rangle|z_0\rangle, \tag{5}$$

where $b^{(0)a,z_0}(t)$, $b_{ls}^{(0)b,z_0}(t)$ and $b_{l_1 l_2\uparrow\downarrow}^{(0)c,z_0}(t)$ are coefficients for the respective states. The superscripts refer to the number of electrons transferred (0 here), the states of the QPC island (as illustrated in figure 2), and the four two-qubit basis states. The subscripts refer to the left electrode states from which electrons tunnel into the islands. Thus each of the terms in $|\Psi_0(t)\rangle$ indicates a state with as few as zero but up to two electrons moved from the left electrode to the QPC island, while no electron is transferred to the right electrode. $|\Psi_1(t)\rangle$ can be expressed as

$$\begin{aligned} |\Psi_1(t)\rangle = \sum_{n=1}^{\infty} \sum_{\substack{z_0=A,\ldots,D \\ \beta_1\cdots\beta_n}} & \left\{ b_{\beta_1\cdots\beta_n}^{(n)a,z_0}(t) + \sum_{ls} b_{ls\beta_1\cdots\beta_n}^{(n)b,z_0}(t) d_s^\dagger c_{ls} \right. \\ & \left. + \sum_{l_1 l_2} b_{l_1 l_2\uparrow\downarrow\beta_1\cdots\beta_n}^{(n)c,z_0}(t) d_\uparrow^\dagger d_\downarrow^\dagger c_{l_1\uparrow} c_{l_2\downarrow} \right\} \otimes \prod_{i=1}^{n} \left(c_{l_i' s_i'}^\dagger c_{r_i' s_i'} \right) |0\rangle|z_0\rangle, \end{aligned} \tag{6}$$

where $\beta_i \equiv (l_i', r_i', s_i')$ represent the left electrode, right electrode, and spin states involved in the transferred electrons. Similarly to the expressions of the coefficients for $|\Psi_0(t)\rangle$, here $b_{\beta_1\cdots\beta_n}^{(n)a,z_0}(t)$, $b_{ls\beta_1\cdots\beta_n}^{(n)b,z_0}(t)$ and $b_{l_1 l_2\uparrow\downarrow\beta_1\cdots\beta_n}^{(n)c,z_0}(t)$ are coefficients for the states with n electrons transferred to the right electrode, and another zero to two electrons moved from the left electrode to the QPC island. The superscripts again refer to the number of transferred electrons (n), the QPC island states, and the qubit basis states.

Substituting this wavefunction into the Schrödinger equation for the whole qubit–QPC system, $i|\dot{\Psi}(t)\rangle = H|\Psi(t)\rangle$ (having set $\hbar = 1$), we obtain a set of algebraic equations for the coefficients in equations (5) and (6). Assuming zero magnetic field and spin-independent electron tunnelling, the density matrix elements can be defined as

$$\rho_{z_1 z_2}^{u_1 u_2}(t) \equiv \sum_{\beta} \int \frac{\mathrm{d}E\,\mathrm{d}E'}{4\pi^2} \tilde{b}_\beta^{u_1,z_1}(E) \tilde{b}_\beta^{u_2,z_2 *}(E) \mathrm{e}^{\mathrm{i}(E-E')t}, \tag{7}$$

where $\tilde{b}_\beta^{u_1,z_1}(E)$ is a Laplace-transformed element of $b_\beta^{u_1,z_1}(t)$ after summing over $\beta = \{0, \beta_1, \beta_2, \cdots, \beta_n, \cdots\}$, the electrode states of transferred electrons as discussed above ('0' corresponds to coefficients in equation (5)).

After a lengthy calculation, we obtain 48 equations for the density matrix elements $\rho_{z_1 z_2}^{u}(t)$, where $u = a, b_\uparrow, b_\downarrow, c$ indicate quantum states of the inter-QPC island (figure 2) as shown in the appendix[3]. Because we assume that there is no magnetic field, $\rho_{z_1 z_2}^{b\uparrow}(t) = \rho_{z_1 z_2}^{b\downarrow}(t)$.

The readout current is obtained as a time derivative of the number of electrons in the island [8]:

$$I(t) = e\Gamma_{\mathrm{R}} \left[\rho^{b\uparrow}(t) + \rho^{b\downarrow}(t) \right] + 2e\Gamma_{\mathrm{R}}' \rho^{c}(t), \tag{8}$$

[3] Compared with the two-island SET detector we considered before [8], where we need 352 equations to describe the coupled qubit–detector system, the number of density matrix equations for the QPC detector is significantly reduced.

where ρ^u given by $\rho^u \equiv \rho^u_{AA} + \rho^u_{BB} + \rho^u_{CC} + \rho^u_{DD}$ is the occupation probability of the particular island state u.

As the difference between $\Gamma^{(+)}_\alpha$ and $\Gamma^{(-)}_\alpha$ increases, the current difference that depends on the difference of qubit states increases as well, while the qubits lose their coherence faster due to the fluctuations in the QPC current, which lead to fluctuations in the qubit energy levels and thus dephasing. We quantify the strength of the measurement by dephasing rates defined as

$$\begin{aligned} \Gamma^\alpha_{\rm d} &\equiv \left(\sqrt{\Gamma^{(+)}_\alpha} - \sqrt{\Gamma^{(-)}_\alpha}\right)^2, \\ \Gamma^{\alpha'}_{\rm d} &\equiv \left(\sqrt{\Gamma^{(+)'}_\alpha} - \sqrt{\Gamma^{(-)'}_\alpha}\right)^2, \end{aligned} \tag{9}$$

where $\alpha = {\rm L}, {\rm R}$. These rates are the coefficients of the off-diagonal density matrix elements of the time-dependent reduced density matrix equations for the qubits. The reduced density matrix elements are

$$\rho_{z_1 z_2} \equiv \rho^a_{z_1 z_2} + \rho^{b\uparrow}_{z_1 z_2} + \rho^{b\downarrow}_{z_1 z_2} + \rho^c_{z_1 z_2}. \tag{10}$$

This definition of dephasing rate is originally introduced by Gurvitz [10] for the case of a single qubit. The dephasing time is taken as coinciding with the measurement time. Compared with [10], where there is a single off-diagonal density matrix element, we cannot define a single dephasing rate because of the complexity of our density matrix equations.

The current of a QPC in the tunnelling regime is very sensitive to the potential variations of the QDs that are set close to the QPC channel [11]. We thus can choose from a wide range of parameters for our QPCs. Here we use a particular set of representative parameters:

$$\Gamma^A_{\rm L} = \Gamma^B_{\rm L} = \Gamma^A_{\rm R} = \Gamma^C_{\rm R} = \Gamma^{(-)} = 0.8\Gamma, \tag{11}$$

$$\Gamma^C_{\rm L} = \Gamma^D_{\rm L} = \Gamma^B_{\rm R} = \Gamma^D_{\rm R} = \Gamma^{(+)} = 1.2\Gamma, \tag{12}$$

which lead to $\Gamma^{\rm L}_{\rm d} = \Gamma^{\rm R}_{\rm d} (\equiv \Gamma_{\rm d}) \sim 0.04\Gamma$ for a typical case (Γ is a tunnelling rate in the absence of the qubits, so the dephasing rate is more than one order of magnitude smaller, corresponding to a relatively weak measurement). We can regard $\Gamma^{-1}_{\rm d}$ as the typical measurement time. Obviously, the qubit dynamics (represented by tunnelling rate Ω) would be able to be detected when $\Omega^{-1} < \Gamma^{-1}_{\rm d}$. Because, in the present setup, the current without qubits saturates in the range of $\sim\Gamma^{-1}$, the time Γ^{-1} would serve as a standard of when measurement started. We can also incorporate the effect of Coulomb interaction by setting $\Gamma^{(\pm)'}_{\rm L} = 0$ as a limiting case of strong on-site Coulomb blockade ($U \to \infty$ in equation (2) so that no double occupation is possible), while for weak Coulomb interaction on the island we can set $\Gamma^{(\pm)'}_\alpha = \Gamma^{(\pm)}_\alpha$ at the limit of $U = 0$.

3. Qubit dynamics without detector

In order to better understand our numerical results and the capability of our QPC detector, it is instructive to first examine the dynamics of both a single qubit and two qubits in the absence of any detector, and discuss how the qubit dynamics is measured by the detector.

We first solve the density matrix equations for a single qubit on the basis of localized single quantum dot states $|\uparrow\rangle$ and $|\downarrow\rangle$:

$$\dot{\rho_{\uparrow\uparrow}} = {\rm i}\Omega(\rho_{\uparrow\downarrow} - \rho_{\downarrow\uparrow}), \tag{13}$$

$$\dot{\rho_{\downarrow\downarrow}} = {\rm i}\Omega(\rho_{\downarrow\uparrow} - \rho_{\uparrow\downarrow}), \tag{14}$$

$$\dot{\rho_{\uparrow\downarrow}} = {\rm i}\Delta\rho_{\uparrow\downarrow} + {\rm i}\Omega(\rho_{\uparrow\uparrow} - \rho_{\downarrow\downarrow}). \tag{15}$$

For the simple case of $\Delta = 0$ (no voltage bias between the two dots so that qubit dynamics is completely determined by the inter-dot tunnel coupling Ω, which corresponds to the optimal operational point in terms of minimum dephasing as discussed in [12]), and starting from one of the localized states $\uparrow$-state ($\rho_{\uparrow\uparrow}(t=0)=1$) or $\downarrow$-state ($\rho_{\downarrow\downarrow}(t=0)=1$), we have

$$\rho_{\uparrow\uparrow}(t) = \rho_{\uparrow\uparrow}(0)\cos^2(\Omega t) + \rho_{\downarrow\downarrow}(0)\sin^2(\Omega t), \tag{16}$$

$$\rho_{\downarrow\downarrow}(t) = \rho_{\downarrow\downarrow}(0)\cos^2(\Omega t) + \rho_{\uparrow\uparrow}(0)\sin^2(\Omega t), \tag{17}$$

$$\rho_{\uparrow\downarrow}(t) = \frac{\mathrm{i}}{2}(\rho_{\uparrow\uparrow}(0) - \rho_{\downarrow\downarrow}(0))\sin(2\Omega t). \tag{18}$$

These solutions dictate that the QPC current should essentially be determined by $\rho_{\uparrow\uparrow}(t) - \rho_{\downarrow\downarrow}(t) = [\rho_{\uparrow\uparrow}(0) - \rho_{\downarrow\downarrow}(0)]\cos 2\Omega t$. The oscillatory component of the QPC current should thus be dominated by a 2Ω component (in the case of $\Delta \neq 0$, $2\sqrt{\Omega^2 + \Delta^2/4}$), and the temporal evolution of the current is intimately related to the initial state.

We can also infer information on the two-qubit product states from the detector current in a similar manner because density matrices of the product states are written as $\rho_{AA}(t) = \rho^{\mathrm{L}}_{\downarrow\downarrow}(t)\rho^{\mathrm{R}}_{\downarrow\downarrow}(t)$ and so on. Here we solve the two-qubit dynamics in the absence of the detector by expanding the density matrix on the basis spanned by the Bell states: $|e_1\rangle = (|\downarrow\downarrow\rangle + |\uparrow\uparrow\rangle)/\sqrt{2}$, $|e_2\rangle = (|\downarrow\downarrow\rangle - |\uparrow\uparrow\rangle)/\sqrt{2}$, $|e_3\rangle = (|\downarrow\uparrow\rangle + |\uparrow\downarrow\rangle)/\sqrt{2}$, and $|e_4\rangle = (|\downarrow\uparrow\rangle - |\uparrow\downarrow\rangle)/\sqrt{2}$ (singlet state). If we assume two identical qubits ($\Omega_{\mathrm{L}} = \Omega_{\mathrm{R}}$ and $\Delta_{\mathrm{L}} = \Delta_{\mathrm{R}}(= \Delta)$), the density matrix equations for the two qubits (without the QPC detector: $\Gamma^{\alpha}_{\mathrm{d}} = 0$) are written as

$$\begin{aligned}
\dot\rho_{e_4e_4} &= 0\\
\dot\rho_{e_2e_2} &= 2\mathrm{i}\Delta(\rho_{e_2e_1} - \rho_{e_3e_2})\\
\dot\rho_{e_2e_4} &= -2\mathrm{i}J\rho_{e_2e_4} - 2\mathrm{i}\Delta\rho_{e_1e_4}
\end{aligned} \tag{19}$$

$$\begin{aligned}
\dot\rho_{e_1e_1} &= 2\mathrm{i}\Omega(\rho_{e_1e_3} - \rho_{e_3e_1}) + 2\mathrm{i}\Delta(\rho_{e_1e_2} - \rho_{e_2e_1})\\
\dot\rho_{e_3e_3} &= -2\mathrm{i}\Omega(\rho_{e_1e_3} - \rho_{e_3e_1})\\
\dot\rho_{e_1e_3} &= -2\mathrm{i}\Omega(\rho_{e_3e_3} - \rho_{e_1e_1}) - 2\mathrm{i}J\rho_{e_1e_3} - 2\mathrm{i}\Delta\rho_{e_2e_3}
\end{aligned} \tag{20}$$

$$\begin{aligned}
\dot\rho_{e_1e_2} &= -2\mathrm{i}\Omega\rho_{e_3e_2} - 2\mathrm{i}\Delta(\rho_{e_1e_1} - \rho_{e_2e_2})\\
\dot\rho_{e_2e_3} &= 2\mathrm{i}\Omega\rho_{e_2e_1} - 2\mathrm{i}J\rho_{e_2e_3} - 2\mathrm{i}\Delta\rho_{e_1e_3}
\end{aligned} \tag{21}$$

$$\begin{aligned}
\dot\rho_{e_3e_4} &= -2\mathrm{i}\Omega\rho_{e_1e_4}\\
\dot\rho_{e_1e_4} &= -2\mathrm{i}\Omega\rho_{e_3e_4} - 2\mathrm{i}J\rho_{e_1e_4} - 2\mathrm{i}\Delta\rho_{e_1e_4}.
\end{aligned} \tag{22}$$

If $\Delta = 0$, which again corresponds to the optimal operational point, the density matrix equations can be classified into four groups (indicated by the four parentheses above). First of all, equations (19) shows that the probabilities in $|e_2\rangle$ and $|e_4\rangle$ states are time independent. On the other hand, according to equation (20), the probabilities in $|e_1\rangle$ and $|e_3\rangle$ states oscillate as a function of $\{\cos(4\Omega^* t), \sin(4\Omega^* t)\}$ ($\Omega^* \equiv \sqrt{\Omega^2 + J^2/4}$). Meanwhile, equations (21) and (22) indicate that the off-diagonal elements $\{\rho_{e_1e_2}, \rho_{e_2e_3}, \rho_{e_3e_4}, \rho_{e_1e_4}\}$ contain $\{\cos(2\Omega^* t), \sin(2\Omega^* t)\}$ type of oscillations. Therefore, the occupation probabilities for the product states, $\rho_{AA} = (\rho_{e_1e_1} + \rho_{e_1e_2} + \rho_{e_2e_1} + \rho_{e_2e_2})/2$, $\rho_{BB} = (\rho_{e_3e_3} + \rho_{e_3e_4} + \rho_{e_4e_3} + \rho_{e_4e_4})/2$, $\rho_{CC} = (\rho_{e_3e_3} - \rho_{e_3e_4} - \rho_{e_4e_3} + \rho_{e_4e_4})/2$, and $\rho_{DD} = (\rho_{e_1e_1} - \rho_{e_1e_2} - \rho_{e_2e_1} + \rho_{e_2e_2})/2$, should all contain $\{\cos(2\Omega^* t), \sin(2\Omega^* t)\}$ oscillations, reconfirming the calculations on single-qubit dynamics at the beginning of this section. Therefore, we should be able to distinguish pure entangled states from pure product states $|A\rangle \sim |D\rangle$ based on whether the detected period of the coherent oscillations is limited to $\{\cos(4\Omega^* t), \sin(4\Omega^* t)\}$ ($|e_1\rangle$ and $|e_3\rangle$) or time independent ($|e_2\rangle$ and $|e_4\rangle$) in the limit of weak interaction between the qubits and the QPCs. Such behaviour is indeed evident in our results, as shown in the following section.

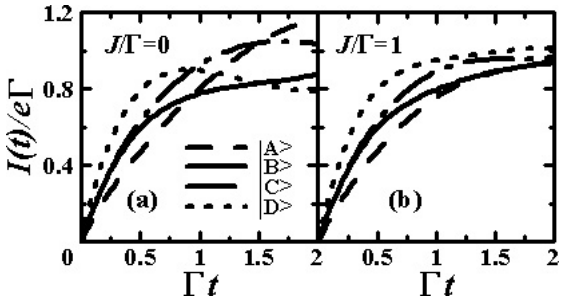

Figure 3. Time-dependent QPC current $I(t)$ of the $U = 0$ case ($\Gamma_\alpha^{(\pm)'} = \Gamma_\alpha^{(\pm)}$) starting from four product qubit states $|A\rangle \sim |D\rangle$ at time $t = 0$. $\Omega_L = \Omega_R = 0.75\Gamma$, $\Gamma_d = 0.04\Gamma$. The two panels refer to two different inter-qubit interaction: (a) $J = 0$, (b) $J = \Gamma$. We can distinguish the four product states in both the $J = 0$ case and the $J = \Gamma$ case. This shows that we can distinguish the four two-qubit product states in a range of inter-qubit coupling strength.

4. Numerical results of QPC detection

In [8], we clarified three major issues regarding the capability of the two-island SET by monitoring its time-dependent readout current: (1) the two-qubit product states (eigenstates in the absence of inter-qubit interaction and inter-dot coupling within each qubit) $|A\rangle \sim |D\rangle$ can be distinguished; (2) pure entangled states and pure product states can be distinguished; (3) the quantum Zeno effect is present in a two-qubit system. In the following we show that similar results are obtained for the serially coupled QPC detector despite its simpler state structure.

Figure 3 shows the time-dependent current at small time $t \sim 0$ in the case of weak Coulomb interaction ($U = 0$) ($\Gamma_\alpha^{(\pm)'} = \Gamma_\alpha^{(\pm)}$) assuming that initially the two qubits are in one of the four product states. To calculate the current when the two-qubit initial state is $|A\rangle$, for example, we set $b^{(0)a,A}(0) = 1$ and the other coefficients to zero in the total wavefunction (equations (5) and (6)), which means that $\rho_{AA}^{aa}(0) = 1$ and other density matrix elements are all zero at $t = 0$. At small t initial state $|A\rangle$ (with both electrons located in the respective lower dots) leads to the strongest suppression of the QPC current, while initial state $|D\rangle$ (with both electrons located in the respective upper dots) leads to the least. States $|B\rangle$ and $|C\rangle$ also produce different QPC currents. The reason is that there is a finite bias between the left and right electrodes, so the current flows only in one direction. Consequently, $|C\rangle$, with the left qubit electron in the upper dot (thus less suppression on current), produces a faster rise in current than $|B\rangle$. Since the product states are not the two-qubit eigenstates, they evolve into superposition states and the corresponding QPC current oscillates. Nevertheless, we can distinguish the four initial product states by the values of the readout current in both $J = 0$ and $J \neq 0$ cases. Hereafter we will focus on the $J = 0$ case. As shown in figure 3, the current differences between the four two-qubit states can be detected before the coherent motion of the qubits changes the two-qubit state as $\Omega t < \pi/4$.

One observation we made for charge qubits measured by an SET detector is that the amplitude of the SET current oscillations corresponding to the pure entangled states are smaller than those of the pure product states [8]. Similar effects are also observed for the QPC detectors here, as indicated in figures 4 and 5. A qualitative reason is that the wavefunctions of the entangled states in the charge qubits extend over both qubits compared to the product states, so the charge distribution of the entangled states is less effective in influencing the readout current. Quantitatively, for instance, equation (19) also dictates that current corresponding to a singlet state should have very weak time dependence. Indeed, figure 4 shows strong differences between QPC currents for the singlet state $|e_4\rangle$ and product state $|B\rangle$: the detector current on

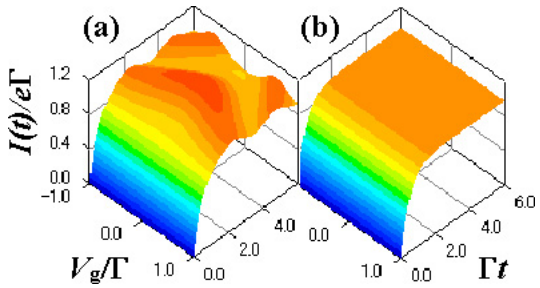

Figure 4. Time evolution of QPC current $I(t)$ corresponding to the product $|B\rangle$ state (panel (a)) and the entangled singlet state $|e_4\rangle$ (panel (b)) when the qubit gate-bias V_g ($=\Delta_L = \Delta_R$) changes. The relevant parameters are chosen as $\Omega_L = \Omega_R = 0.75\Gamma$, $J = 0$, $U = 0$ and $\Gamma_d = 0.04\Gamma$. The $I(t)$ for the product state (a) explicitly reflects the coherent oscillations of the qubit states, while those for the entangled state are rather uniform.

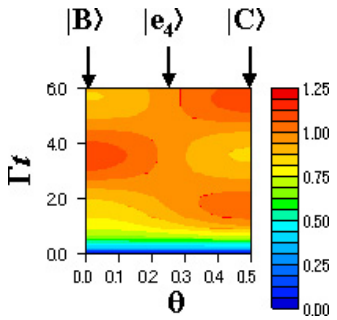

Figure 5. A contour plot of the time evolution of QPC current for states ranging between $|B\rangle$ state and $|C\rangle$ state through singlet state $|e_4\rangle$ (see text). The current for the "general" singlet state shows uniform characteristics when it is close to the exact singlet state $|e_4\rangle$ as $|\theta \pm \pi/4| \leqq \pi/12$. The chosen parameters are similar to what we have before: $\Omega_L = \Omega_R = 0.75\Gamma$, $J = 0$, $V_g = 0$, $U = 0$, and $\Gamma_d = 0.04\Gamma$. In addition, the current for $|B\rangle$ and $|C\rangle$ has a oscillatory component of frequency $2\Omega = 1.5$.

the singlet state is essentially a smoothly rising function of time, while the current for the product state has an oscillatory component of frequency $\sim 2\Omega$ at $V_g = 0$. We obtained similar current behaviours for other entangled states and product states, where the peaks of the coherent oscillations in the other product states are shifted as inferred from figure 3. These features hold as long as the entangled states are close to any of the Bell states, $|e_1\rangle, \sim |e_4\rangle$. Figure 5 shows the time-dependent current of the generalized singlet state $\cos\theta|{\downarrow\uparrow}\rangle + e^{i\varphi}\sin\theta|{\uparrow\downarrow}\rangle$ in the range of $\varphi = \pi$, $0 \leqq \theta \leqq \pi/2$. We found that the uniformity of the readout current holds approximately up to $|\theta \pm \pi/4| \leqq \pi/12$, which is remarkably robust (similar to the case of charge qubits measured by SET detectors [8]). In addition, in figure 5, the current for product states $|B\rangle$ and $|C\rangle$ also contain oscillatory components of frequency $\sim 2\Omega$.

An interesting aspect in studying quantum measurement is to explore the backaction of the measurement apparatus on the qubits. In this context, the quantum Zeno effect refers to the phenomenon that a continuous measurement slows down transitions between qubit quantum states due to the collapse of the qubit wavefunction into observed states. This phenomenon might be useful in quantum computation because it preserves the results of quantum calculations for a longer period of time [13]. Figure 6 demonstrates the quantum Zeno effect for two qubits measured by the QPC, where the initial state is chosen to be the $|D\rangle$

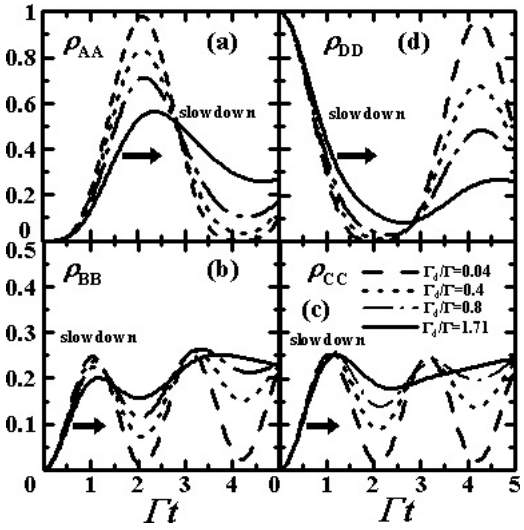

Figure 6. Time dependence of $\rho_{AA}(t)$, $\rho_{BB}(t)$, $\rho_{CC}(t)$ and $\rho_{DD}(t)$ for the $U = 0$ case ($\Gamma_\alpha^{(\pm)'} = \Gamma_\alpha^{(\pm)}$), starting from $\rho_{DD}(t = 0) = 1$, for different measurement strengths (in terms of Γ_d). Here the intra-qubit tunnelling rates are $\Omega_\mathrm{L} = \Omega_\mathrm{R} = 0.75\Gamma$, and there is no interaction between the qubits: $J = 0$. As measurement strength Γ_d increases, the coherent motions of qubits slow down, which is a clear evidence of the quantum Zeno effect.

state ($\rho_{DD}(t = 0) = 1$). As the measurement strength increases (Γ_d increases), the oscillations of the density matrix elements of the two qubits are delayed, which is a clear evidence of the slowdown described by the Zeno effect, under the condition that other origins of decoherence are neglected.

In general, increasing measurement strength (i.e. the coupling strength between the qubits and the QPCs) leads to faster entanglement between the qubits and the measuring apparatus, so that measurement leads to projection of qubit states into product states. Therefore, stronger measurement strength destroys entangled qubit states more rapidly. This is in contrast to the product states, for which the quantum Zeno effect is observed (figure 6) [13]. We use the concept of concurrence [14] to quantify two-qubit entanglement and calculate concurrence in the presence of increasing measurement strength. Figure 7 shows the effect of measurement on the singlet state, demonstrating that stronger measurement (in the form of larger Γ_d) degrades the entanglement (in terms of concurrence) more rapidly. As seen from equations (13)–(15) and from (19)–(22), product states and entangled states discussed here are generally not two-qubit eigenstates even in the absence of the detector, and thus could evolve into each other through the time-dependent coherent oscillations. Strong detection enhances the mixing of these states and makes it more difficult to infer the qubit states from the detector current. Figures 8(a) and (b) show the time-dependent currents of $|e_4\rangle$ (singlet state) and $|e_3\rangle$ state as functions of increasing measurement strength. Without the detector, the singlet $|e_4\rangle$ state should be time independent according to equation (19), and $|e_3\rangle$ should show 4Ω oscillation according to equation (20). Figures 8(a) and (b) indicate these characteristics in the weak measurement case $\Gamma_\mathrm{d} < 0.04\Gamma$, which is also the case that we discussed concerning figure 4. In this region, we would be able to distinguish the different behaviours of entangled states and product states. However, as the strength of measurement increases, the detector current starts to acquire other oscillatory components, which means that both states are mixing with other states after $t = 0$. Figure 9 is a time-dependent diagonal matrix element $\rho_{e_4e_4}$ of the singlet

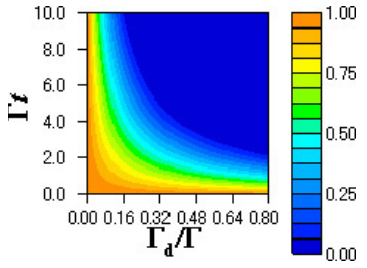

Figure 7. Time-dependent concurrence of a two-qubit state starting from a singlet state $|e_4\rangle$ as a function of the dephasing rate Γ_d in the same parameter region as figure 5. At $t = 0$ and $\Gamma_d = 0$, the concurrence takes a value of 1 and rapidly decreases to zero for large dephasing rates.

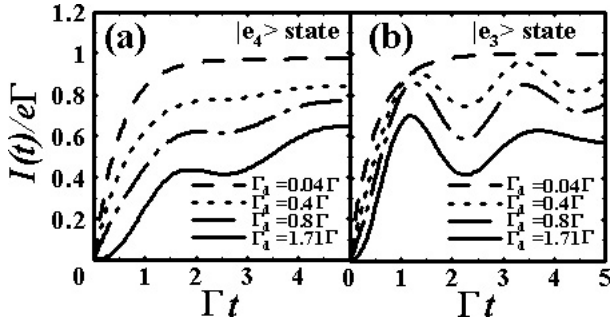

Figure 8. Time-dependent currents for $|e_4\rangle$ (singlet state) (panel (a)) and $|e_3\rangle$ state (panel (b)) state, when the dephasing rate Γ_d is changed with $\Delta = 0$. The parameters are the same as those in figure 5. At $\Gamma_d < 0.04\Gamma$, (a) presents the proof of time independence of the singlet state in equation (19), and (b) shows the proof of the 4Ω oscillation of equation (20).

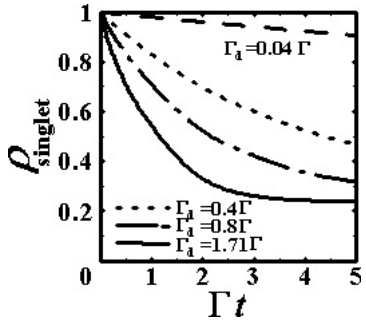

Figure 9. Time-dependent diagonal density matrix element for the singlet state $\rho_{\text{singlet}} \equiv \rho_{e_4e_4}$, when the dephasing rate Γ_d is changed with $\Delta = 0$. The parameters are the same as those in figure 5. Without the detector, that is the case of no decoherence by measurement, $\rho_{\text{singlet}} = 1$. This figure shows that the two-qubit state begins to include states other than the singlet states, resulting in the oscillation of the current in figure 8(a) when Γ_d becomes large.

state. This figure also shows that the singlet state mixes with other states as the strength of measurement increases.

In the case of a strong Coulomb interaction so that $\Gamma_L^{(\pm)'} = 0$, we have obtained similar results, except that the magnitude of the average current is reduced by half because the on-site Coulomb interaction closes one transmission channel. This is different from the coupled SET

detector we studied before, where current uniformity in finite-U model is more persistent than in the infinite-U model, because the internal degrees of freedom in the two-island SET allow a redistribution of electrons between the islands. Here there is only one island with three island states (unoccupied, singly occupied, and doubly occupied, shown in figure 2). The much simpler internal dynamics of these states is insufficient to cause any large change in the QPC current when Coulomb interaction is accounted for.

5. Discussion

In our study so far we have demonstrated that two-charge-qubit state information can be clearly revealed by the transient current variations in a serially coupled QPC charge detector. The key question now is whether such current evolutions are experimentally observable. A single shot measurement cannot differentiate the small currents here—the current calculated is an ensemble average over many identically prepared samples, and as indicated in figures 3, 4 and 8, we require the measurement of ns scale dynamics of a pA current when we take Γ in the order of 100 MHz. Instead, the recently developed pulsed measurement technique [1, 3, 15–18] is a perfect approach to detect the QPC current. Specifically, the qubits and the QPCs are repeatedly prepared in an identical initial state at the beginning of a cycle (defined as $t = 0$). The system is then allowed to evolve for a particular time period τ. At $t = \tau$ the QPC is turned off by shifting the level of the inter-QPC QD off resonance, so that sequential tunnelling is not allowed between the two QPCs (while charges in the QPCs can still relax into the leads). From $t = \tau$ to $t_{\rm prep}$ (the end of the current cycle), operations are needed to reinitialize the coupled qubits and the two QPCs. At $t = t_{\rm prep}$ the whole cycle starts again. Throughout these cycles, the external circuit used for measuring the current remains on, so the data acquisition time can be as long as needed. The current I_m measured as such can then be used to determine the charge transferred (between the two QPCs) during τ (which is the same as the charge transferred during each cycle $t_{\rm prep}$): $\Delta Q(\tau) = I_m(\tau)t_{\rm prep}$, and the QPC current at τ can be deduced as $I_{\rm QPC}(\tau) = {\rm d}\Delta Q(\tau)/{\rm d}\tau$. Notice that what we have given here is a series of simple guidelines, which need to be properly adapted/modified for a particular experimental system.

One issue we have been trying to address in this study is to compare the measurement capability of a QPC detector and an SET detector. In terms of the theoretical descriptions of the qubit–detector interaction, the major difference between the QPC detector studied here and the SET detector in [8] is that we model each QPC by a tunnel junction, so that the QPC–qubit interaction directly modifies strength of tunnelling, while in [8], the SET–qubit interaction influences both the SET island state energy and the island-lead tunnelling. Despite these differences, our numerical results showed that the current through the coupled QPC exhibits behaviours similar to those of the two-island SET current in many respects, such as in distinguishing the different qubit product states, in distinguishing the Bell-type entangled states from the product states, and in the observation of the quantum Zeno effect for the qubit product states. Stronger differences between QPC and SET detectors do appear when the qubit–detector interaction strength increases. The measurement current of the detector that has a larger number of internal degrees of freedom (the two-island SET) seems to be able to describe more elaborate quantum states of the two qubits. For example, the SET current can clearly distinguish the four product states shown in [8], while with the present QPC detector the current shows a simpler structure and smaller differences for the different qubit states. Qualitatively, the tunnelling rate of a QPC is generally larger than that of an SET, which corresponds to shorter dwelling time for the QPC (in the present study the dwelling time for QPCs is effectively taken to be zero). This difference essentially originates from the simpler structure of a QPC compared to an SET.

In the present study we obtained the density matrix equations under the condition that the voltage bias between the left and right electrodes is sufficiently large such that the left–right symmetry is broken and the transmission of electrons from the right electrode to the left can be neglected as shown in equations (5) and (6), which makes calculation process much simpler. In order to calculate the QPC conductance or differential conductance, which would provide more information for some experiments, we have to improve our formulation such that the transmission of electrons to the inverse direction is included. An approach that can properly deal with these low bias situations is still in development.

Our configuration of the qubit–QPC coupling scheme can be straightforwardly extended to $N(N > 2)$-qubit detection. However, it depends strongly on the sensitivity of the current readout circuit such that the 2^N states can be differentiated [6], and is thus better suited for only a small number of qubits. In any case, the key objective of the present study is to obtain two-qubit information directly and dynamically, not to invent a general detector for a multi-qubit system, for which other configurations such as a typical one-detector-per-qubit setup are probably more suitable and have to be further studied both experimentally and theoretically [16–20]. Furthermore, we have considered an ideal measurement process in the present study. In a more realistic situation, imperfections such as gate operation errors [21], charge fluctuations around the qubit–QPC systems [22], and phonons have to be considered. These imperfections could seriously reduce the sensitivity of a measuring device. Thus more detailed analysis for the coupled multiqubit–detector system needs to be carried out in the future to further clarify these issues.

6. Conclusion

We have solved master equations and described various time-dependent measurement processes of two charge qubits by two serially coupled QPCs. The current through the QPCs is shown to be an effective means to measure the results of quantum calculations and the presence of entangled states. Two-qubit dynamics is studied analytically and it is found that period of coherent oscillation depends on their initial state. Our results thus show that the serially coupled QPC can be an effective detector of two-qubit states of a pair of (coupled) charge qubits.

Acknowledgments

We thank N Fukushima, S Fujita, J Koga, R Ohba, M Ueda, T Fujisawa and S Ishizaka for valuable discussion. Also, XH thanks support by NSA, LPS, ARDA, and ARO of the US.

Appendix. Derivation of density matrix equations

Here we display all the density matrix equations of the qubit–QPC system. The density matrix equations can be classified according to the electronic states of the QPC island (see figure 2) and qubit states ($z_1, z_2 = A, B, C, D, s = \uparrow, \downarrow$).

$$\frac{\mathrm{d}\rho^a_{z_1z_2}}{\mathrm{d}t} = (\mathrm{i}[J_{z_2} - J_{z_1}] - [\Gamma^{z_1}_{\mathrm{L}} + \Gamma^{z_2}_{\mathrm{L}}])\rho^a_{z_1z_2} - \mathrm{i}\Omega_{\mathrm{R}}(\rho^a_{g_r(z_1),z_2} - \rho^a_{z_1,g_r(z_2)}) - \mathrm{i}\Omega_{\mathrm{L}}(\rho^a_{g_l(z_1),z_2} - \rho^a_{z_1,g_l(z_2)}) + \sqrt{\Gamma^{z_1}_{\mathrm{R}}\Gamma^{z_2}_{\mathrm{R}}}(\rho^{b\uparrow}_{z_1z_2} + \rho^{b\downarrow}_{z_1z_2}), \tag{A.1}$$

$$\frac{\mathrm{d}\rho^{b_s}_{z_1z_2}}{\mathrm{d}t} = \left(\mathrm{i}[J_{z_2} - J_{z_1}] - \frac{\Gamma_{\mathrm{L}}^{z_1'} + \Gamma_{\mathrm{L}}^{z_2'} + \Gamma_{\mathrm{R}}^{z_1} + \Gamma_{\mathrm{R}}^{z_2}}{2}\right)\rho^{b_s}_{z_1z_2} - \mathrm{i}\Omega_{\mathrm{R}}(\rho^{b_s}_{g_r(z_1),z_2} - \rho^{b_s}_{z_1,g_r(z_2)})$$
$$- \mathrm{i}\Omega_{\mathrm{L}}(\rho^{b_s}_{g_l(z_1),z_2} - \rho^{b_s}_{z_1,g_l(z_2)}) + \sqrt{\Gamma_{\mathrm{L}}^{z_1}\Gamma_{\mathrm{L}}^{z_2}}\rho^{a}_{z_1z_2} + \sqrt{\Gamma_{\mathrm{R}}^{z_1'}\Gamma_{\mathrm{R}}^{z_2'}}\rho^{c}_{z_1z_2}, \tag{A.2}$$

$$\frac{\mathrm{d}\rho^{c}_{z_1z_2}}{\mathrm{d}t} = (\mathrm{i}[J_{z_2} - J_{z_1}] - [\Gamma_{\mathrm{R}}^{z_1'} + \Gamma_{\mathrm{R}}^{z_2'}])\rho^{c}_{z_1z_2} - \mathrm{i}\Omega_{\mathrm{R}}(\rho^{c}_{g_r(z_1),z_2} - \rho^{c}_{z_1,g_r(z_2)})$$
$$- \mathrm{i}\Omega_{\mathrm{L}}(\rho^{c}_{g_l(z_1),z_2} - \rho^{c}_{z_1,g_l(z_2)}) + \sqrt{\Gamma_{\mathrm{L}}^{z_1'}\Gamma_{\mathrm{L}}^{z_2'}}(\rho^{b\uparrow}_{z_1z_2} + \rho^{b\downarrow}_{z_1z_2}), \tag{A.3}$$

where

$$\Gamma_{\mathrm{L}}^{A} = \Gamma_{\mathrm{L}}^{B} = \Gamma_{\mathrm{L}}^{(+)}, \qquad \Gamma_{\mathrm{L}}^{C} = \Gamma_{\mathrm{L}}^{D} = \Gamma_{\mathrm{L}}^{(-)},$$
$$\Gamma_{\mathrm{R}}^{A} = \Gamma_{\mathrm{R}}^{C} = \Gamma_{\mathrm{R}}^{(+)}, \qquad \Gamma_{\mathrm{R}}^{B} = \Gamma_{\mathrm{R}}^{D} = \Gamma_{\mathrm{R}}^{(-)},$$
$$\Gamma_{\mathrm{L}}^{A'} = \Gamma_{\mathrm{L}}^{B'} = \Gamma_{\mathrm{L}}^{(+)'}, \qquad \Gamma_{\mathrm{L}}^{C'} = \Gamma_{\mathrm{L}}^{D'} = \Gamma_{\mathrm{L}}^{(-)'},$$
$$\Gamma_{\mathrm{R}}^{A'} = \Gamma_{\mathrm{R}}^{C'} = \Gamma_{\mathrm{R}}^{(+)'}, \qquad \Gamma_{\mathrm{R}}^{B'} = \Gamma_{\mathrm{R}}^{D'} = \Gamma_{\mathrm{R}}^{(-)'},$$

and

$$J_A = \Delta_{\mathrm{L}} + \Delta_{\mathrm{R}} + J, \qquad J_B = \Delta_{\mathrm{L}} - \Delta_{\mathrm{R}} - J,$$
$$J_C = -\Delta_{\mathrm{L}} + \Delta_{\mathrm{R}} - J, \qquad J_D = -\Delta_{\mathrm{L}} - \Delta_{\mathrm{R}} + J.$$

$g_l(z_i)$ and $g_r(z_i)$ are introduced for the sake of notational convenience and represent relationships between different two-qubit states in the equations for the density matrix elements:

$$g_r(A) = B, \quad g_l(A) = C, \quad g_r(B) = A, \quad g_l(B) = D,$$
$$g_r(C) = D, \quad g_l(C) = A, \quad g_r(D) = C, \quad g_l(D) = B.$$

References

[1] Nakamura Y, Pashkin Y A and Tsai J S 1999 *Nature* **398** 786
Nakamura Y, Pashkin Y A, Yamamoto T and Tsai J S 2002 *Phys. Rev. Lett.* **88** 047901
[2] Makhlin Y, Schön G and Shnirman A 2001 *Rev. Mod. Phys.* **73** 357
[3] Fujisawa T, Austing D G, Tokura Y, Hirayama Y and Tarucha S 2002 *Nature* **419** 278
Fujisawa T, Austing D G, Tokura Y, Hirayama Y and Tarucha S 2002 *Phys. Rev. Lett.* **88** 236802
Fujisawa T, Tokura Y and Hirayama Y 2001 *Phys. Rev.* B **63** 081304
Hayashi T, Fujisawa T, Cheong H D, Jeong Y H and Hirayama Y 2003 *Phys. Rev. Lett.* **91** 226804
[4] van der Wiel W G, Franceschi S De, Elzerman J M, Fujisawa T, Tarucha S and Kouwenhoven L P 2003 *Rev. Mod. Phys.* **75** 1
Tarucha S, Austing D G, Honda T, van der Hage R J and Kouwenhoven L P 1996 *Phys. Rev. Lett.* **77** 3613
[5] Pashkin Yu A, Yamamoto T, Astafiev O, Nakamura Y, Averin D V and Tsai J S 2003 *Nature* **421** 823
Yamamoto T, Pashkin Y A, Astafiev O, Nakamura Y and Tsai J S 2003 *Nature* **425** 941
[6] Tanamoto T 2001 *Phys. Rev.* A **64** 062306
Tanamoto T 2000 *Phys. Rev.* A **61** 022305
[7] Korotkov A N 2002 *Phys. Rev.* A **65** 052304
Ruskov R and Korotkov A N 2003 *Phys. Rev.* B **67** 241305
[8] Tanamoto T and Hu X 2004 *Phys. Rev.* B **69** 115301
[9] Aleiner I L, Wingreen N S and Meir Y 1997 *Phys. Rev. Lett.* **79** 3740
[10] Gurvitz S A and Prager Ya S 1996 *Phys. Rev.* B **53** 15932
Gurvitz S A 1997 *Phys. Rev.* B **56** 15215
[11] Field M, Smith C G, Pepper M, Ritchie D A, Frost J E F, Jones G A C and Hasko D G 1993 *Phys. Rev. Lett.* **70** 1311
[12] Vion D, Aassime A, Cottet A, Joyez P, Pothier H, Urbina C, Esteve D and Devoret M H 2002 *Science* **296** 886
[13] Zurek W H 1984 *Phys. Rev. Lett.* **53** 391

Duan L M and Guo G C 1998 *Phys. Rev.* A **57** 2399
[14] Hill S and Wootters W K 1997 *Phys. Rev. Lett.* **78** 5022
Wootters W K 1998 *Phys. Rev. Lett.* **80** 2245
[15] Schoelkopf R J, Wahlgren P, Kozhevnikov A A, Delsing P and Prober D E 1998 *Science* **280** 1238
[16] Gardelis S, Smith C G, Cooper J, Ritchie D A, Linfield E H, Jin Y and Pepper M 2003 *Phys. Rev.* B **67** 073302
Rushforth A W, Smith C G, Godfrey M D, Beere H E, Ritchie D A and Pepper M 2004 *Phys. Rev.* B **69** 113309
[17] Cain P A, Ahmed H and Williams D A 2002 *J. Appl. Phys.* **92** 346
Cain P A, Ahmed H and Williams D A 2001 *Appl. Phys. Lett.* **78** 3624
[18] Potok R M, Folk J A, Marcus C M, Umansky V, Hanson M and Gossard A C 2003 *Phys. Rev. Lett.* **91** 016802
[19] Elzerman J M, Hanson R, Greidanus J S, Willems van Beveren L H, Franceschi S De, Vandersypen L M K, Tarucha S and Kouwenhoven L P 2004 *Phys. Rev.* B **67** 161308
Zhang L-X, Matagne P, Leburton J P, Hanson R and Kouwenhoven L P 2004 *Phys. Rev.* B **69** 245301
[20] DiCarlo L, Lynch H J, Johnson A C, Childress L I, Crockett K, Marcus C M, Hanson M P and Gossard A C 2004 *Phys. Rev. Lett.* **92** 226801
[21] Hu X and Das S S 2002 *Phys. Rev.* A **66** 012312
[22] Itakura T and Tokura Y 2003 *Phys. Rev.* B **67** 195320